Magnet Design of the 150 mm Aperture Low-β Quadrupoles for the High Luminosity LHC

P. Ferracin, G. Ambrosio, M. Anerella, F. Borgnolutti, R. Bossert, D. Cheng, D.R. Dietderich, H. Felice, A. Ghosh A. Godeke, S. Izquierdo Bermudez, P. Fessia, S. Krave, M. Juchno, J. C. Perez, L. Oberli, G. Sabbi, E. Todesco, and M. Yu

***Abstract*— The High Luminosity LHC (HL-LHC) project is aimed at studying and implementing the necessary changes in the LHC to increase its luminosity by a factor five. Among the magnets that will be upgraded are the 16 superconducting low-β quadrupoles placed around the two high luminosity interaction regions (ATLAS and CMS experiments). In the current baseline scenario, these quadrupole magnets will have to generate a gradient of 140 T/m in a coil aperture of 150 mm. The resulting conductor peak field of more than 12 T will require the use of Nb_3Sn superconducting coils. We present in this paper the HL-LHC low-β quadrupole design, based on the experience gathered by the US LARP program, and, in particular, we describe the support structure components to pre-load the coils, withstand the electro-magnetic forces, provide alignment and LHe containment, and integrate the cold mass in the LHC IRs.**

***Index Terms*—High Luminosity LHC, Interaction Regions, Low-β Quadrupoles, Nb_3Sn magnets.**

I. Introduction

The present Interaction Regions (IR) of the Large Hadron Collider [1] implement four single-aperture quadrupole magnets (called low-β or inner triplet quadrupoles) based on Nb-Ti superconducting technology [2]. These quadrupoles present two different designs, both with an aperture of 70 mm and an operating gradient of 205 T/m (see Fig. 1, first line from the top): the 6.6 m long quadrupole MQXA [3] developed by KEK, and the 5.7 m long quadrupole MQXB built at FNAL [4]. MQXA features a four-layer coil wound with an 11 mm wide cable, clamped by 10 mm thick spacers, and pre-loaded by yoke laminations keyed at the mid-plane [5]. MQXB uses a two-layer coil wound with a 15.4 mm wide cable and contained by free-standing collars [6], [7]. With the current IR design, the LHC is expected to reach its nominal luminosity L_0 of 10^{34} cm^{-2} s^{-1} and to provide ~300–500 fb^{-1} of integrated luminosity at 6.5–7 TeV per beam by 2021.

Manuscript received July 16, 2013. The HiLumi LHC Design Study is included in the High Luminosity LHC project and is partly funded by the European Commission within the Framework Programme 7 Capacities Specific Programme, Grant Agreement 284404.

P. Ferracin, J.C. Perez, S. Izquierdo Bermudez, P. Fessia, M. Juchno, and E. Todesco are with CERN, CH-1211 Geneva 23, Switzerland (e-mail: paolo.ferracin@cern.ch).

G. Ambrosio, R. Bossert, S. Krave, and M. Yu with Fermi National Accelerator Laboratory, Batavia, IL 80510 USA.

M. Anerella and A. Ghosh are with BNL, Upton, NY 11973-5000, USA.

F. Borgnolutti, D. Cheng, D.R. Dietderich, H. Felice, A. Godeke, and G. Sabbi are with Lawrence Berkeley National Lab, Berkeley, CA 94720, USA.

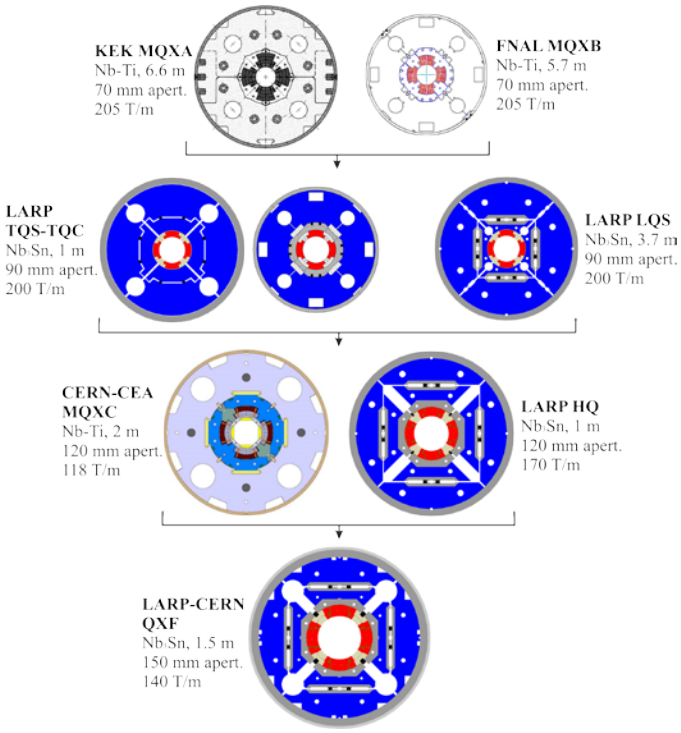

Fig. 1. LHC low-β Quadrupole overview.

Since 2004, four US laboratories (BNL, FNAL, LBNL and SLAC) have been working, within the framework of the DOE-funded LHC Accelerator Research Program (LARP), on the development of high-gradient Nb_3Sn quadrupoles for future upgrades of the LHC IRs [8]. In the early stages of the program, increasing the quadrupole aperture from 70 to 90 mm, while maintaining the same field gradient of 200 T/m, was identified as the best option to bring the accelerator to the ultimate luminosity of 2-3 · 10^{34} cm^{-2} s^{-1} [9].

With this goal, LARP launched the design and fabrication of the Nb_3Sn Technology Quadrupole (TQ) model series [10] (see Fig. 1, second line from the top). Whereas all the models featured two-layer coils wound with a 10 mm wide cable around a 90 mm aperture, two different designs for the mechanical structure were investigated. The TQC models used a MQXB-type support structure (defined as collar-based structure), where the coil pre-load and support against electro-magnetic forces was provided by a combination of collars and yoke laminations [11]. The TQS models adopted a structure with an external shell pre-loaded with water-pressurized bladders (so-called shell-based structure) [12]. Both designs

reached the target gradient of 200 T/m [13], [14]. In parallel, the 3.7 m long model LQS [15], [16], a length scale-up of the TQS design, was developed, and, by reaching the target gradient of 200 T/m [17], served as a proof-of-principle for long Nb_3Sn cos2θ coils and long shell-based structures.

In 2008, CERN approved a two-phase approach for the upgrade of the LHC accelerator complex. According to the plan, the Phase-I luminosity upgrade included the upgrade of the current low-β triplets to enable the operation of the LHC at the ultimate luminosity. This effort resulted in the design [19] and the construction [20] of the Nb-Ti quadrupole magnet MQXC (see Fig. 1, third line from the top) by a CERN-CEA collaboration. With an aperture of 120 mm and an operating gradient of 118 T/m, the magnet was characterized by a two-layer coil wound with the 15 mm wide cables from the LHC main dipoles and it used self-supporting collars. In two consecutive tests MQXC reached the nominal gradient [21], [22]. Simultaneously to the development of MQXC, LARP started working on a Nb_3Sn quadrupole for the "Phase-II" luminosity upgrade. The choice was to develop HQ, a quadrupole with the same 120 mm aperture as MQXC but a nominal gradient of 170 T/m. The HQ adopted a 15 mm wide cable and a support structure similar to the LQ design with the addition of aluminum bolted collars for coil alignment purposes [23], [24]. It reached the target gradient in both the first (HQ01 [25]-[27]) and the second series (HQ02 [28]).

In the summer of 2012, as a baseline scenario for the HiLumi LHC Luminosity, it was finally decided to choose a low-β quadrupole design with an aperture of 150 mm and Nb_3Sn based technology. The goal is to increase the peak luminosity by a factor of 5 and reach 3000 fb^{-1} of integrated luminosity [29], [30]. The quadrupole magnet, called QXF, will be developed by a collaborative effort between LARP and CERN. The purpose of this paper is to give an overview of the QXF design and parameters, with particular emphasis on its support structure and mechanical behavior. A description of the magnetic design is reported in [31], while the results of the quench protection analysis are described in [32].

II. Magnet Design and Parameters

A. Conductor and Cable

The QXF cable is composed of 40 strands with a diameter of 0.85 mm. Both Bruker Powder-in-tube (PIT) conductor, featuring 192 filaments, and OST Restacked-Rod-Process (RRP) conductors, with 108/127, 132/169, and 144/169 stack, will be used. For both conductors, the design parameters for the project assume a non-Cu J_c of 2450 (1400) A/mm^2 at 12 (15) T applied magnetic field and 4.2 K as measured on a standard ITER barrel, a Cu/Sc ratio of 1.2, and a RRR>150. This leads to a minimum measured virgin strand critical current of 632 (361) A at 12 (15) T applied magnetic field. The resulting minimum performance of the wire in the cable can be calculated using LARP standard parameterizations as described in [33], by applying a 0.429 T/kA self-field correction for the ITER barrel and assuming a 5% cabling degradation, which results in a strand current of 631 (354) A at 12 (15) T total magnetic field and 4.2 K.

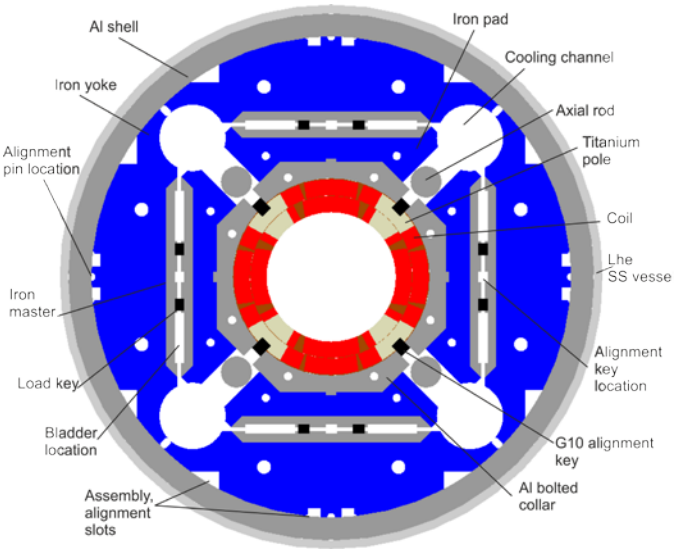

Fig. 2. QXF magnet cross-section.

The cable R&D was focused on maximizing mechanical stability and minimizing the number of sheared sub-elements and the critical current cabling degradation. Table I shows the cable parameters at the end of the first iteration. The cable will be insulated with braided S2 glass with silane sizing and with a target thickness at 5 MPa of 0.150 mm. A stainless steel core 25 microns thick is incorporated in the cable to reduce dynamic effects. Its width, currently of 12.7 mm, will be tailored to achieve the required performance. The optimization of the cable parameter is still in process, and, depending on the results, second iteration parameters may be defined. For computation and tooling design purposes, the increase of cable cross-section during reaction has been included. The width and the thickness were increased by respectively 2% and 4.5%, consistently with measurements collected during the HQ program [26].

TABLE I
Conductor and Cable Parameters

Parameter	Unit	
Strand diameter	mm	0.85
Fabrication process		RRP, PIT
Number of SC filaments		108-132-144,192
RRR		>150
Cu/SC		1.2
Non-Cu J_c (12 T, 4.2 K), no self-field corr.	A/mm^2	2450
Non-Cu J_c (15 T, 4.2 K), no self-field corr.	A/mm^2	1400
Number of strands		40
Cabling degradation	%	5
Cable bare width (before/after HT)	mm	18.150/18.513
Cable bare thickness (before/after HT)	mm	1.525/1.594
Keystone angle	Deg.	0.55
Insulation thickness per side at 5 MPa	mm	0.150

B. Magnet cross-section

The design of QXF is basically a scale-up in radius of HQ [34]. The cross-section of the magnet is shown in Fig. 2. The design relies on a system of water-pressurized bladders and keys to apply a partial pre-stress to coil-pack and to pre-tension to aluminum shell at room temperature. During the assembly, the pressurized bladders compress the coil-pack and allow shimming the load keys, placed between the iron yoke

and the iron pad, with interference shims. To facilitate the assembly and room temperature loading operations, keys and bladders are installed between the iron masters, which provide a flat surface to the bladders and alignment between yoke and pad. The final pre-stress is applied during the cool-down phase, when the tensioned aluminum shell compresses the structure components because of its high thermal contraction. The pre-load is set to prevent the coil from detaching from the pole during powering to 90% of the current limit I_{ss}. The alignment of the coil with respect to the structure is ensured by a G10 key inserted in the coil poles and by thick-lamination bolted collars. The collars have only an alignment function: they do not provide pre-load and, since they are made of aluminum, they intercept only a minimal fraction of the compressive force provided by the shell. With respect to the HQ, additional accelerator features have been added to the design, such as 77 mm diameter cooling holes in the yoke, slots and cut-outs in the outer surface of the yoke to facilitate assembly, handling, and alignment of the structure, and an external stainless steel shell to provide LHe containment. The magnet parameters are given in Table II: at the nominal conditions, the magnet operates at 82% of I_{ss}.

TABLE II
COIL AND MAGNET PARAMETERS

Parameter	Unit	
Clear aperture diameter	mm	150
Magnet (LHe vessel) outer diameter	mm	630
No. turns in layer 1/2 (octant)		22/28
Operational temperature T_{op}	K	1.9
Nominal gradient G_{nom}	T/m	140
Nominal current I_{nom}	kA	17.5
Nominal conductor peak field B_{nom}	T	12.1
Short sample gradient G_{nom} at 1.9 K	T/m	168
Short sample current I_{ss} at 1.9 K	kA	21.2
Short sample cond. peak field B_{ss} at 1.9 K	T	14.5
Stored energy density in straight sect. at I_{nom}	MJ/m	1.32
Differential inductance at I_{nom}	mH/m	8.2
F_x / F_y (per octant) at I_{nom}	MN/m	+2.65 / -3.87
F_z (whole magnet) at I_{nom}	MN	1.4

III. MECHANICAL ANALYSIS

A 2D numerical model of the QXF structure was developed using ANSYS® to simulate its behavior. The numerical analysis and the geometry optimization were performed taking into account the pressurization of bladders, the insertion of the interference shim, the cool-down, and powering. The computations were carried out according to the following set of requirements: 1) to ensure that pre-load is maintained to both coil layers during all magnet operations, in particular by keeping the pole turns in contact with the winding poles with a pressure ≥2 MPa at the mid-radius up to 90% of I_{ss}; 2) to minimize the coil peak stress during room-temperature loading and after cool-down: indicative target values are 100 MPa at 293 K and 150-200 MPa at 1.9 K; 3) to maintain the stress in the support structure components within the material limits (see Table III), and to limit the principal stress σ_1 of the iron at 1.9 K to 200 MPa in order to prevent brittle fracture; 4) to maintain the bladder pressure below 50 MPa while ensuring a 100 μm clearance with respect to the nominal shim thickness.

TABLE III
MATERIAL STRESS LIMITS

Material	Yield Strength (MPa)	
	293 K	4.2 K
Al 7075	480	690
SS 316 LN	350	1050
NITRONIC 40	350	1240
MAGNETIL	180	720
Ti 6Al 4V	830	1650

The mechanical analysis was focused on 1) the determination of the optimal dimensions of the different structural components, 2) the computation of the stress distribution inside the coil, 3) the investigation of the effect of mechanical deformations on field quality, and finally 5) the impact of a welded LHe vessel on the structure stress.

A. Dimension of the components

Among the different parameters to be optimized, the crucial ones concerning the coil pre-load were 1) bladder size and interference shim thickness, which set the room temperature pre-load, 2) shell thickness, which determines the stress increase during cool-down, and 3) load key position, which defines the coil stress distribution. In addition, other parameters related to size and shape of the support structure components were adjusted to obtain a further fine tuning of the stress state in the structure. As a result, 19 mm thick collars and 21 mm thick pads were chosen. The optimal level of pre-load was obtained with the use of a 27 mm thick aluminum shell and interference shims of 600 μm. The total clearance of 600+100 μm, needed for the insertion of the keys, was obtained by 58 mm wide bladders pressurized at 40 MPa. The coil peak stress was minimized by positioning interference keys at 25 mm from the mid-plane.

B. Coil Stress

The azimuthal stress evolutions in the coil inner and outer layers are given in Fig. 3 and Fig. 4. The round, square, and diamond markers indicate the azimuthal stresses respectively at the mid-radius of the pole turn (center of the turn), at the mid-radius of the mid-plane turn, and the peak azimuthal stress in the whole layer. The values are plotted as a function of the different phases, i.e. bladder inflation, interference shim insertion and bladder deflation, cool-down and powering up to 155 T/m.

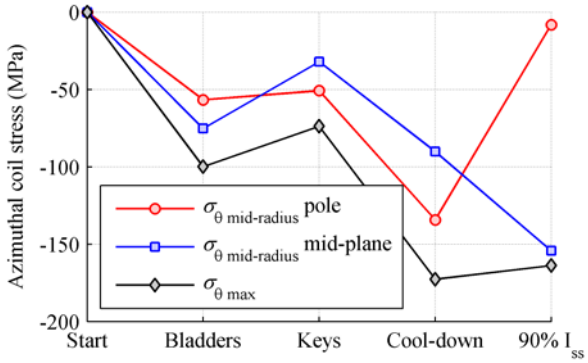

Fig. 3. Azimuthal stress in the coil inner layer from assembly to excitation: mid-radius of the pole turn (square markers), mid-radius of the mid-plane turn (round markers), and the whole layer peak stress (diamond markers).

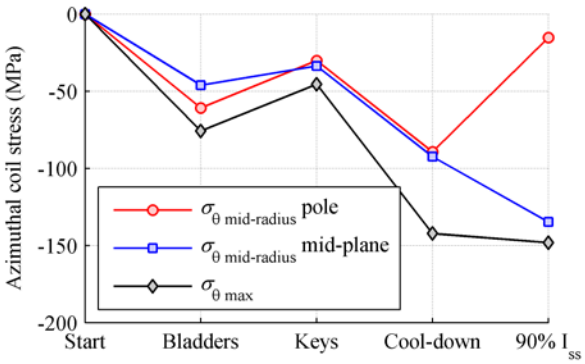

Fig. 4. Azimuthal stress in the coil outer layer from assembly to excitation: mid-radius of the pole turn (square markers), mid-radius of the mid-plane turn (round markers), and the whole layer peak stress (diamond markers).

In the first step, bladders are inflated to 40 MPa to create a 0.7 mm interference for the shim insertion. In these conditions, a maximum coil stress of 100 MPa is reached in the inner layer. Then, the insertion of a 0.6 mm thick shim and deflation of the bladder result in a "spring-back" that reduces the coil stresses in both layers. As expected, an increase of pre-load is observed at 1.9 K, when the peak stress rises to 180 MPa in the inner layer. Finally, when electro-magnetic forces are applied, the pole stress reduces, but a compression of about 5-10 MPa is maintained up to 90% of I_{ss}.

C. Effect of Coil Deformation on Field Quality

The results of the 2D structural analysis in ANSYS were used to investigate the effects of the coil deformation on the field quality. The study was carried out by importing the coil displacement map extracted from the ANSYS solution into the 2D magnetic model implemented in Roxie. The displacement map corresponds to the state of the coil after the room temperature pre-load, the cool-down and the excitation to 140 T/m, and it is estimated with respect to the design coil geometry at room temperature without any pre-load. The computed displacements were applied to every strand of the magnetic model and a harmonic analysis was performed with the displaced strand distribution. The deformation of the iron yoke was not taken into account during this analysis.

TABLE IV
AVERAGE DISPLACEMENT OF COIL-BLOCKS SIDES

Layer	Block	Δr_1	Δr_2	$\Delta l_{\theta 1}$	$\Delta l_{\theta 2}$
		mm	mm	mm	mm
Inner	Mid-plane	-0.290	-0.351	0.000	-0.047
Inner	Pole	-0.315	-0.367	-0.043	-0.044
Outer	Mid-plane	-0.360	-0.420	0.000	-0.041
Outer	Block	-0.370	-0.433	-0.043	-0.050

Table IV shows the average displacements of the coil block sides estimated by the mechanical model. In particular, Δr_1 and Δr_2 are the average radial displacements of the inner and outer radius of the block, and $\Delta l_{\theta 1}$ and $\Delta l_{\theta 2}$ the average azimuthal displacement of the top and bottom side of the block. The results of the mechanical analysis indicate a radial displacement of the blocks of -0.3 to -0.4 mm and an azimuthal disaplcement of -0.04 to -0.05 mm. The output of the numerical magnetic model showed a change in the normalized b_6 harmonic of 0.75 units and a negligible change of other allowed harmonics such as b_{10} and b_{14} (see Table V). The offset of the b_6 is mostly caused by the azimuthal coil deformation, which results from the pre-load applied to the structure during the assembly and the structure contraction during the cool-down phase. As expected for quadupole magnets, the deformations resulting from the electro-magnetic forces have a negligible effect on the b_6.

The numerical harmonic analysis was validated analytically with the use of the formulas of the multipoles generated by a block of a sector coil [35], [36]. As shown in Table V, although the absolute value of the b_6 harmonic calculated by analytical formulas presents a discrepancy of about 4 units due to the simplification of the coil geometry with a sector coil, good agreement is found on the effect of the coil deformation.

TABLE V
RESULTS OF NUMERICAL AND ANALYTICAL FIELD QUALITY ANALYSIS

	Numerical			Analytical		
	Undef.	Def.	Δ	Undef.	Def.	Δ
b_6 (units)	0.26	1.01	0.75	4.50	5.36	0.86
b_{10} (units)	0.22	0.20	-0.02	2.10	2.16	0.06

D. LHe Containment

The shell-based structure of QXF will feature an external aluminum shell segmented in about 1 m long sections. This option was already adopted and successfully tested in two 4 m long Nb_3Sn magnets, the LRS [37], [38] and LQ [39], [40] series. Since the segmented shell cannot provide LHe containment, QXF will feature a stainless steel shell, 10 mm thick, outside the aluminum cylinder. The stainless steel shell will also provide alignement between the magnets within the same cryostat. Two options are currently under investigation: a single inertia tube slid around the aluminium shell, or two half-shells tightly welded around the magnets. In the second case, the welding should provide enough pre-load at room temperature to guarantee contact between the two shells also after cool-down. According to the 2D finite element model, the segmented magnet structure contracts radially about 100 μm more than the stainless-steel shell. To compensate for this effect, it was calculated that the LHe vessel pre-tension provided by the welding should be 70 MPa, resulting in a 10 MPa peak stress increase in the components at 293 K.

IV. CONCLUSION AND PLANS

In this paper we describe the design of the QXF, the Nb_3Sn quadrupole magnet aimed at upgrading the inner triplet magnets of the LHC IRs. QXF has an aperture of 150 mm and an operating gradient of 140 T/m, which, according to strand properties, corresponds to 82% of its current limits at the operational temperature of 1.9 K. The design features a double layer coil wound with an 18 mm wide cable and supported by a shell-based structure. The structure is capable of maintaining the coil under compression up to 90% of I_{ss} with a peak stress below 200 MPa. The plan foresees the start of the coil fabrication for the short model program (SQXF) in 2014 and the test of the first short model in 2015. The development of long magnets (MQXF and LQXF) both at CERN and by LARP will follow, with the goal of installing the new low-β Nb_3Sn quadrupole magnets in the LHC by 2022.

REFERENCES

[1] O. Bruning, *et al*., LHC Design Report, CERN 2004-003 (2004).

[2] S. Feher, *et al*., "Production and Installation of the LHC Low-β Triplets," *IEEE Trans. Appl. Supercond.*, vol. 16, no. 2, pp. 437-440, June 2006.

[3] A. Yamamoto, *et al*., "Production and Measurement of the MQXA Series of LHC Low-β Insertion Quadrupoles", *IEEE Trans. Appl. Supercond.*, vol. 15, no. 2, pp. 1084-1089, June 2005.

[4] S. Feher, *et al*., "Test results of LHC interaction regions quadrupoles produced by Fermilab," *IEEE Trans. Appl. Supercond.*, vol. 15, no. 2, pp. 1090–1093, June 2005.

[5] T. Nakamoto, *et al*., "Fabrication and Mechanical Behavior of a Prototype for the LHC Low-β Quadrupole Magnets", *IEEE Trans. Appl. Supercond.*, vol. 12, no. 1, pp. 174-177, March 2002.

[6] N. Andreev, *et al.*, "Quench Performance and Mechanical Behavior of the First Fermilab-Built Prototype High Gradient Quadrupole for the LHC Interaction Regions", *IEEE Trans. Appl. Supercond.*, vol. 12, no. 1, pp. 59-62, March 2002.

[7] N. Andreev, *et al*., "Mechanical Design and Analysis of LHC Inner Triplet Quadrupole Magnets at Fermilab", *IEEE Trans. Appl. Supercond.*, vol. 10, no. 1, pp. 115-118, March 2000.

[8] S. A. Gourlay, *et al.*, "Magnet R&D for the US LHC Accelerator Research Program", *IEEE Trans. Appl. Supercond.*, vol. 16, no. 2, pp. 324-327, June 2006.

[9] T. Sen, J. Strait, and A. V. Zlobin, Proceedings of the 2001 Particle Accelerator Conference, Chicago, Illinois, pp. 3421-3423.

[10] P. Ferracin, "LARP Nb_3Sn Quadrupole Magnets for the LHC Luminosity Upgrade", *AIP Conf. Proc*,. 1218, pp. 1291-1300, 2010.

[11] R. C. Bossert, *et al*., "Development of TQC01, a 90 mm Nb_3Sn Model Quadrupole for LHC Upgrade Based on SS Collar," *IEEE Trans. Appl. Supercond.*, vol. 16, no. 2, pp. 370-373, June 2006.

[12] S. Caspi, *et al.*, "Design and Analysis of TQS01, a 90 mm Nb3Sn Model Quadrupole for LHC Luminosity Upgrade Based on a Key and Bladder Assembly," *IEEE Trans. Appl. Supercond.*, vol. 16, no. 2, pp. 358-361, June 2006.

[13] R. C. Bossert, *et al.*, "Fabrication and Test of LARP Technological Quadrupole Models of TQC Series," *IEEE Trans. Appl. Supercond.*, vol. 16, no. 2, pp. 370-373, June 2006.

[14] H. Felice, *et al*., "Test results of TQS03: a LARP shell-based Nb_3Sn quadrupole using 108/127 conductor," *Journal of Physics: Conference Series* 234, 032010, 2010.

[15] G. Ambrosio, *et al.*, "Development and Coil Fabrication for the LARP 3.7-m Long Nb_3Sn Quadrupole," *IEEE Trans. Appl. Supercond.*, vol. 19, no. 3, pp. 1231-1234, June 2009.

[16] P. Ferracin, *et al.*, "Fabrication and Test of a 3.7 m Long Support Structure for the LARP Nb_3Sn Quadrupole Magnet LQS01," *IEEE Trans. Appl. Supercond.*, vol. 19, no. 3, pp. 1683-1686, June 2009.

[17] G. Ambrosio, *et al.*, "Test Results and Analysis of LQS03 Third Long Nb_3Sn Quadrupole by LARP," *IEEE Trans. Appl. Supercond.*, vol. 23, no. 3, 4002204, June 2013.

[18] R. Ostojic, "LHC Interaction Region Upgrade – Phase I," LHC Project Report 1094, August 2008.

[19] S. Russenchuck, *et al.*, "Design Challenges for a Wide-Aperture Insertion Quadrupole Magnet ," *IEEE Trans. Appl. Supercond.*, vol. 21, no. 3, pp. 1674-1677, June 2011.

[20] G. A. Kirby, *et al.*, "Engineering Design and Manufacturing Challenges for a Wide-Aperture, Superconducting Quadrupole Magnet," *IEEE Trans. Appl. Supercond.*, vol. 22, no. 3, 4001804, June 2012.

[21] G. A. Kirby, *et al*., "Testing Results for Nb-Ti, 120-mm-Aperture, Low-β Quadrupole Models for the LHC High-Luminosity Insertion," *IEEE Trans. Appl. Supercond.*, vol. 23, no. 3, 4002105, June 2013.

[22] G. A. Kirby, *et al.*, "LHC IR Upgrade Nb-Ti, 120mm Aperture Model Quadrupole Test Results at 1.8K," *IEEE Trans. Appl. Supercond.* 24 submitted for publication.

[23] S. Caspi, *et al.*, "Design of HQ—A High Field Large Bore Nb_3Sn Quadrupole Magnet for LARP," *IEEE Trans. Appl. Supercond.*, vol. 19, no. 3, pp. 1235-1238, June 2009.

[24] S. Caspi, *et al.*, "Design of a 120 mm Bore 15 T Quadrupole for the LHC Upgrade Phase II," *IEEE Trans. Appl. Supercond.*, vol. 20, no. 3, pp. 144-147, June 2010.

[25] S. Caspi, *et al.*, "Test Results of 15 T Nb_3Sn Quadrupole Magnet HQ01 with a 120 mm Bore for the LHC Luminosity Upgrade," *IEEE Trans. Appl. Supercond.*, vol. 21, no. 3, pp. 1854-1857, June 2011.

[26] H. Felice, *et al*., "Impact of Coil Compaction on Nb_3Sn LARP HQ Magnet," *IEEE Trans. Appl. Supercond.*, vol. 22, no. 3, pp. 4001904, June 2012.

[27] H. Bajas, *et al*., "Cold Test Results of the LARP HQ Nb_3Sn Quadrupole Magnet at 1.9 K," *IEEE Trans. Appl. Supercond.*, vol. 23 no. 3, pp. 4002606, June 2013.

[28] G. Chlachidze, *et al.*, "Performance of HQ02, an optimized version of the 120 mm Nb3Sn LARP quadrupole," *IEEE Trans. Appl. Supercond.* 24 submitted for publication.

[29] E. Todesco, *et al.*, "Design Studies for the Low-Beta Quadrupoles for the LHC Luminosity Upgrade," *IEEE Trans. Appl. Supercond.*, vol. 23 no. 3, pp. 4002405, June 2013.

[30] E. Todesco, *et al.*, "A first baseline for the magnets in the high luminosity LHC insertion regions," *IEEE Trans. Appl. Supercond.* 24 submitted for publication.

[31] F. Borgnolutti, *et al.*, "Magnetic design optimization of a 150 mm aperture Nb3Sn low-beta quadrupole for the HiLumi LHC," *IEEE Trans. Appl. Supercond.* 24 submitted for publication.

[32] G. Manfreda, *et al.*, "Quench protection study of the Nb_3Sn low-beta quadrupole for the LHC luminosity upgrade (HiLumi-LHC)," *IEEE Trans. Appl. Supercond.* 24 submitted for publication.

[33] A. Godeke, *et al*., "A Review of Conductor Performance for the LARP High-Gradient Quadrupole Magnets," accepted for *Supercond. Sci. Techn.* 2013.

[34] P. Ferracin, *et al.*, "Mechanical Behavior of HQ01, a Nb_3Sn Accelerator-Quality Quadrupole Magnet for the LHC Luminosity Upgrade," *IEEE Trans. Appl. Supercond.*, vol. 22 no. 3, pp. 4901804, June 2012.

[35] R. Meuser, "Magnetic Field for a Thick cos nθ Winding Engineering Note M5254," Lawrence Berkeley National Lab., 1978.

[36] L. Rossi and E. Todesco, "Electromagnetic design of superconducting quadrupoles," *Phys. Rev. ST Accel. Beams* 9, 102401 2006.

[37] P. Ferracin, *et al.*, "Assembly and Test of a Support Structure for 3.6 m Long Nb_3Sn Racetrack Coils," *IEEE Trans. Appl. Supercond.*, vol. 18, no. 2, pp. pp. 167-171, June 2008.

[38] J. F. Muratore, *et al.*, "Test Results of LARP 3.6 m Nb_3Sn Racetrack Coils Supported by Full-Length and Segmented Shell Structures," *IEEE Trans. Appl. Supercond.*, vol. 19, no. 3, pp. 1212-1215, June 2009.

[39] P. Ferracin, *et al.*, "Assembly and Loading of LQS01, a Shell-Based 3.7 m Long Nb_3Sn Quadrupole Magnet for LARP," *IEEE Trans. Appl. Supercond.*, vol. 20, no. 3, pp. 279-282, June 2010.

[40] G. Ambrosio, *et al.*, "Test Results of the First 3.7 m Long Nb_3Sn Quadrupole by LARP and Future Plans," *IEEE Trans. Appl. Supercond.*, vol. 21, no. 3, pp. 1858-1861, June 2011.